

The FRB Domain of mTOR: NMR Solution Structure and Inhibitor Design^{†,‡}Marilisa Leone,[§] Kevin J. Crowell,[§] Jinhua Chen, Dawoon Jung, Gary G. Chiang, Sina Sareth, Robert T. Abraham,^{||} and Maurizio Pellecchia*

Cancer Research Center, Burnham Institute for Medical Research, 10901 North Torrey Pines Road, La Jolla, California 92037

Received May 17, 2006; Revised Manuscript Received July 5, 2006

ABSTRACT: The mammalian target of rapamycin (mTOR) is a protein that is intricately involved in signaling pathways controlling cell growth. Rapamycin is a natural product that binds and inhibits mTOR function by interacting with its FKBP–rapamycin-binding (FRB) domain. Here we report on the NMR solution structure of FRB and on further studies aimed at the identification and characterization of novel ligands that target the rapamycin binding pocket. The biological activity of the ligands, and that of rapamycin in the absence of FKBP12, was investigated by assaying the kinase activity of mTOR. While we found that rapamycin binds the FRB domain and inhibits the kinase activity of mTOR even in the absence of FKBP12 (in the low micromolar range), our most potent ligands bind to FRB with similar binding affinity but inhibit the kinase activity of mTOR at much higher concentrations. However, we have also identified one low-affinity compound that is also capable of inhibiting mTOR. Hence, we have identified compounds that can directly mimic rapamycin or can dissociate the FRB binding from the inhibition of the catalytic activity of mTOR. As such, these ligands could be useful in deciphering the complex regulation of mTOR in the cell and in validating the FRB domain as a possible target for the development of novel therapeutic compounds.

The phosphatidylinositol 3-kinase-related kinase mTOR¹ plays a critical role in cell growth regulation (1). In mammalian cells, mTOR participates in two protein complexes, one termed mTORC1, which is rapamycin-sensitive, and the other termed mTORC2, which is rapamycin-insensitive. Though many of the details by which each of these mTOR-containing complexes regulate cell signaling have yet to be elucidated, several aspects of mTORC1 function are known, including its kinase activity (2, 3), its function in sensing branched chain amino acid levels (4), and its activity as a regulator of translation initiation (5, 6). Functional studies of the mTORC1 complex have been greatly facilitated by the use of the natural product rapamycin, a bacterially derived macrolide ester, which inhibits mTORC1 function through a poorly defined mechanism. In particular, rapamycin treatment of cells can lead to growth arrest (7), downregulation of protein synthesis (8), and upregulation of mRNA degradation (9).

mTOR has recently been of interest in cancer research (10), and rapamycin is currently undergoing clinical trials for a variety of cancer treatments (11, 12).

Early evidence indicated that rapamycin binds mTOR at a region termed the FRB domain (FKBP12–rapamycin-binding), only after simultaneous interaction with the FKBP12 protein. However, it has been found that rapamycin is able to bind FRB even in the absence of FKBP12, albeit with a lower affinity (13). Such an observation is not unexpected on the basis of the examination of the X-ray crystal structure of the FKBP12–rapamycin–FRB ternary complex (14, 15). In this structure, it is obvious that while rapamycin has many significant interactions with both protein partners, FKBP12 and FRB only make contact at a few locations (15). This fact was key in the original hypothesis of how rapamycin bound to mTOR and exerted its biological function, as it was thought that FKBP12 was indispensable for the binding of rapamycin to FRB. In hindsight, a seed of doubt about this notion is planted with a comparison of the geometry of free rapamycin in solution (16) to that while bound to FRB. Such a comparison shows that rapamycin has virtually the same 3D structure, whether it is bound to FRB. Therefore, it seems counterintuitive to expect that rapamycin alone could not bind to FRB. One possibility that cannot be excluded, however, is that binding of rapamycin to FKBP12 induces somehow a change in the charge distribution in the compound that results in an increased affinity of the FKBP12–rapamycin complex for FRB. To provide additional insights into the role of the FRB domain in modulating the various activities of mTOR, we sought to identify novel small molecules that directly target the FRB domain. Structural and functional studies of the FRB domain in solution and in complex with these compounds are discussed.

[†] Financial support was obtained thanks to NIH Grants CA052995 (M.P. and G.G.C.) and CA102583 (M.P.).

[‡] FRB structures have been deposited in the Protein Data Bank as entry 2GAQ.

* To whom correspondence should be addressed: Burnham Institute for Medical Research, 10901 N. Torrey Pines Rd., La Jolla, CA 92037. Phone: (858) 646-3159. Fax: (858) 713-9925. E-mail: mpellecchia@burnham.org.

[§] These authors contributed equally to this work.

^{||} Current address: Wyeth Research, 401 N. Middletown Rd., Pearl River, NY 10960.

¹ Abbreviations: mTOR, mammalian target of rapamycin; FRB, FKBP–rapamycin-binding; FKBP, FK506-binding protein; HSQC, heteronuclear single-quantum coherence spectroscopy; NOESY, nuclear Overhauser effect spectroscopy; TOCSY, total correlation spectroscopy; rmsd, root-mean-square deviation; 1D, one-dimensional; 2D, two-dimensional; 3D, three-dimensional.

Our studies resulted in novel molecular tools that can be used to further investigate the role of mTOR in the cell and to validate the FRB domain as a target for possible novel drug design.

MATERIALS AND METHODS

Expression and Purification of Recombinant FRB. The basic procedure for the expression of FRB from Luria Broth (LB) and its subsequent purification has been described previously (14). However, recombinant FRB is expressed in both soluble and insoluble forms in a ratio of approximately 3:7. To optimize the yield of FRB, especially for isotopically enriched samples, purification involved refolding of the insoluble fraction. First, the pellets containing the insoluble inclusion bodies were washed three times in alkaline buffer ($\text{NaHCO}_3/\text{Na}_2\text{CO}_3$, pH 10) followed by centrifugation (16 000 rpm in an SS-34 rotor) for 30 min. Following washing steps, the inclusion bodies were solubilized in 6 M guanidine-HCl (Gdn-HCl) in PBS by adding approximately 10 mL of buffer per liter of cell culture. Prior to performing the refolding, we centrifuged and filtered (0.45 μm) the solution to remove insoluble material.

Refolding was accomplished by a combination of rapid dilution and dialysis. First, the denatured GST-FRB protein was added dropwise to a refolding buffer containing arginine (300 mM), phosphate (20 mM), NaCl (500 mM), DTT (1 mM), and sucrose (10%) at neutral pH. The GST-FRB protein was added at a rate of approximately 0.5 mL/min under constant stirring at 4 °C, to a volume of refolding buffer (approximately 300 mL) for 20–30 mL of GST-FRB solution. The mixture was stirred overnight for at least 16 h followed by centrifugation to remove precipitated material. Concentration using an Amicon stirred cell was used to reduce the volume to less than 50 mL. To remove those components that are not desirable for NMR spectroscopy (Gdn-HCl, arginine, sucrose, and excess salt), extensive dialysis against PBS and DTT was carried out. Precipitated material was removed by centrifugation and filtration.

The resulting supernatant (and the original lysis supernatant) was purified by standard GST affinity chromatography using a GE-Amersham 5 mL GSTrap column connected to an AKTA-Prime purification system. Elution was accomplished with 10 mM reduced glutathione, and the eluted GST-FRB protein was subjected to thrombin cleavage by adding approximately 5 mg of thrombin to the GST-FRB protein and dialyzing the mixture against 5 L of PBS and DTT for 24–48 h at 4 °C. An additional 2–3 mg of thrombin was added after cleavage had proceeded for 16–24 h to improve the yield of cleaved FRB to approximately 60%. Pure FRB was isolated from the cleavage mixture by passing the cleavage reaction mixture through a S-100 gel filtration column pre-equilibrated with PBS and DTT, indicating a monomeric species.

For uniform ^{15}N labeling, 0.5 g of $^{15}\text{NH}_4\text{Cl}$ was used per liter of medium. Uniformly doubly labeled (^{15}N and ^{13}C) FRB was produced using 0.5 g of $^{15}\text{NH}_4\text{Cl}$ and 2 g of [^{13}C]glucose per liter of medium. A selective [^{15}N]glycine/serine (Gly/Ser) FRB sample was prepared by using individual amino acids instead of $^{15}\text{NH}_4\text{Cl}$. All amino acids were used at concentrations of 100 mg/L of medium, and the labeling was accomplished using [^{15}N]Gly. The serine labeling is a result of scrambling from Gly during protein biosynthesis.

Virtual Docking. Molecular models were built using Sybyl 6.9 (TRIPOS) and energy-minimized by using the routine MAXIMIN. Initial docking studies with a subset (30 000 compounds) of the Chembridge (San Diego) DiverSet collection (50 000 compounds) were performed with FlexX (17) as implemented in Sybyl 6.9 by using the 3D structure of FRB in complex with a rapamycin and FKBP12 (15). For each compound, 10 solutions were generated and compounds were ranked according to CSCORE (18) which included drug score (19), chemscore (20), and Gold score (21) functions. After visual inspection and calculation of intermolecular hydrogen bonds, a total of 56 compounds were selected for experimental verification by NMR as we have recently described (22).

NMR Spectroscopy. All NMR spectra were acquired on either a 500 or 600 MHz Bruker Avance spectrometer equipped with a Bruker TXI probe. All 1D ^1H experiments were carried out with samples containing unlabeled FRB at a concentration of 0.05 mM. Typical acquisition parameters included a $\pi/2$ pulse of 10 μs , 16K acquisition points, a sweep width of 14 ppm, a recycle delay of 1.5 s, and water suppression based on the Watergate sequence (23). For the 2D ^1H – ^{15}N HSQC (24) experiments, typical experimental parameters included 9 and 39 μs $\pi/2$ pulses for ^1H and ^{15}N , respectively, 2K and 128 acquisition points in the direct and indirect dimensions, respectively, sweep widths of 11 and 30 ppm in the direct and indirect dimensions, respectively, and a recycle delay of 1 s. For experiments using the selective Gly/Ser-labeled FRB, reduced sweep widths of 10 and 16 ppm were used for ^1H and ^{15}N , respectively, with 64 indirect acquisition points. 3D ^{15}N -filtered NOESY and TOCSY experiments were typically carried out with 1K, 40, and 160 acquisition points in the three dimensions (indirect ^{15}N on F_2), with NOESY mixing times of 75–150 ms and TOCSY spin-lock times of 50–80 ms. For the triple-resonance experiments, typical ^{13}C , experimental parameters included a 12 μs $\pi/2$ pulse, 80 indirect acquisition points, and a sweep width of 80 ppm with the ^{13}C carrier placed at approximately 45 ppm.

Spectra for resonance assignments [HNCA (25), 3D ^{15}N -resolved ^1H – ^1H NOESY-HSQC (26), 3D ^{15}N -resolved ^1H – ^1H TOCSY-HSQC (27), and 2D ^1H – ^1H NOESY (28)] were recorded at 10 °C.

Structure Calculations and Analysis. Distance constraints for structure calculations were obtained from two NOESY experiments: a 3D ^{15}N -resolved ^1H – ^1H NOESY-HSQC spectrum (100 ms mixing time) and a 2D ^1H – ^1H NOESY spectrum (100 ms mixing time). NOE cross-peaks were manually integrated with XEASY (29). DYANA (30) was used to transfer NOE intensities into upper distance limits (an inverse sixth-power peak volume–distance relationship and an inverse fourth-power function were used for the backbone and side chains, respectively). Angle constraints were also generated with DYANA by using the $\text{C}\alpha$ chemical shift. Structure calculations were initiated from 100 random conformers. The 20 structures with the lowest DYANA target function were further refined by means of energy minimization using the Gromos96 implementation of Swiss-Pdb Viewer (31). Structures were analyzed with MOLMOL (32) and PROCHECK-NMR (33).

In Vitro Kinase Activity Assay. The details of this particular assay have been described previously (34). Following

resuspension of the cells in lysis buffer [50 mM Tris-HCl (pH 7.4), 100 mM NaCl, 50 mM β -glycerophosphate, 10% glycerol (w/v), 0.02% Tween 20 (w/v), 1 mM EDTA, 10 μ g/mL aprotinin, 1 μ g/mL pepstatin A, 10 μ g/mL leupeptin, 2 mM phenylmethanesulfonyl fluoride, 20 nM microcystin-LR, and 25 mM NaF] and sonication, mTOR was immunoprecipitated using 2 μ g of anti-mTOR antibody per 500 μ g of total protein from the cell lysate. Following incubation for 1 h at 4 °C, a slurry of 50% protein A Sepharose was added, followed by incubation for 30 min at 4 °C and centrifugation to isolate the immunoprecipitated mTOR. This protein was washed with lysis buffer, a high-salt buffer, and finally a kinase assay buffer prior to being used in the assay. The mTOR substrate used here, a GST-tagged version of p70S6K (GST-p70S6K), was expressed and purified as described previously (34). The immune complex kinase reaction was carried out by first resuspending the immunoprecipitated mTOR in a kinase reaction buffer [10 mM HEPES (pH 7.4), 50 mM NaCl, 50 mM β -glycerophosphate, 10% (w/v) glycerol, 10 mM MnCl_2 , and 1 mM DTT], followed by addition of 1 μ g of substrate. The reaction was initiated by adding 10 μ Ci of [γ - 32 P]ATP per reaction, and ATP to a concentration of 10 μ M. Reaction mixtures were incubated for 20 min at 30 °C, and the reactions were quenched with an equal volume of 2 \times SDS-PAGE sample buffer. Visualization of the results of the kinase assays was accomplished by SDS-PAGE on a gradient gel (6 to 15%), followed by electrophoretic transfer to an Immobilon-P membrane. The substrate-containing portion of the membrane was exposed to X-ray film for autoradiography.

RESULTS AND DISCUSSION

NMR Solution Structure of the FRB Domain of mTOR. The process of resonance assignment was carried out at 10 °C due to the sample instability at higher temperatures. Starting from the previously published backbone resonance assignments for this protein at 25 °C (13), we identified side chain protons by comparing 3D ^{15}N -resolved ^1H - ^1H NOESY-HSQC (26) and 3D ^{15}N -resolved ^1H - ^1H TOCSY-HSQC (27) spectra. The acquisition of spectra at lower temperatures allowed us to assign additional resonances with respect to the one previously reported for the same protein construct (13). Very recently, the complete resonance assignments at 25 °C for the FRB domain of mTOR have been reported, but the authors used a protein construct (longer amino acid sequence and His tag) different from the one used in our studies (35).

The FRB solution structure was calculated with DYANA (30) by using a set of 723 distance constraints (181 intraresidue, 198 short-range, 194 medium-range, and 150 long-range). In addition, 56 H-bond constraints (28 upper and 28 lower distance limits), derived from H-D exchange experiments, were included in the calculation as well as 123 angle constraints. Starting from 100 randomly generated structures, we chose 19 conformers which better satisfied the experimental constraints [i.e., lower values of the target function (Table 1)] as being representative of the FRB solution structure and further analyzed them (Figure 1A). In the average NMR structure, as generated with MOLMOL, four α -helical segments can be identified (α 1, W2023–F2039; α 2, V2044–E2059; α 3, L2078–K2090; and α 4, V2094–K2113) (Figure 1B). In analogy with the previously

Table 1: Structural Statistics for FRB Conformers

constraints	
no. of NOE upper distance limits	723
no. of dihedral angle constraints	123
residual target function (\AA^2)	2.56 ± 0.66
no. of residual NOE violations $>0.2 \text{ \AA}$	2
maximum (\AA)	0.39 ± 0.04
energies (kJ/mol)	
total	-4124 ± 84
van der Waals	-2477 ± 62
electrostatic	-3221 ± 73
atomic pairwise rmsd ^a (\AA)	
backbone atoms	0.68
heavy atoms	1.39

^a Only residues encompassing secondary structure elements (i.e., 2023–2039, 2044–2059, 2078–2090, and 2094–2113) were used for rmsd calculations.

reported crystal structures of FRB (15), the four helices pack together forming a four-helix bundle (Figure 1A,B).

The root-mean-square deviation (rmsd) calculated for the secondary structure elements is reported in Table 1. The overall high precision of the structures is reduced by the limited number of constraints used for some residues in the third helix for which problems in the resonance assignments were encountered (i.e., amino acids L2078–E2080 and W2084–Y2088). The rmsd values for backbone and heavy atoms are in fact 0.53 and 1.22 \AA , respectively, if residues in helix α 3 are excluded. Structures were analyzed with PROCHECK-NMR which indicated that 74.0% of the residues are included in the most favored region of the Ramachandran map, 25.5% fall within the allowed regions, and only 0.5% is in the disallowed regions.

The NMR conformer with the fewest constraint violations (structure number 1) was used to compare the solution and X-ray structures of FRB in its unbound form [PDB entry 1AUE (36)] and FRB in complex with rapamycin and FKBP12 [PDB entry 1FPA (14)] (Figure 1C). The pairwise rmsd values on the backbone of the secondary structure elements, as identified in the average NMR structure (residues W2023–F2039, V2044–E2059, L2078–K2090, and V2094–S2112), are 1.50 and 1.51 \AA between the solution and crystal structures of the unbound and bound forms of FRB, respectively (Figure 1C). If residues L2065–D2077 are included in the calculations, the rmsd values are 1.81 and 1.82 \AA , respectively. These residues form distorted helical turns at the beginning of helix α 3 in both crystal structures, while they are disordered in the NMR structure. From these comparisons, it appears evident that the 3D fold of the solution and crystal structures of FRB is very similar as well as the packing of the helices. Differences between the NMR solution and X-ray structures can be found in the intrinsic disordered regions such as the loops which connect the helices and in the N-terminal region of helix α 3.

The surface around the rapamycin binding pocket also appears to be very similar in the NMR and X-ray structures. However, as expected, side chains in the rapamycin binding pocket are not well-defined in the NMR structure. Therefore, we decided to use the X-ray structure of FRB and the resonance assignments for this domain to identify and characterize the binding of potential rapamycin mimics.

Identification of Novel FRB Ligands. As a means of identifying potential small molecule ligands that bind FRB

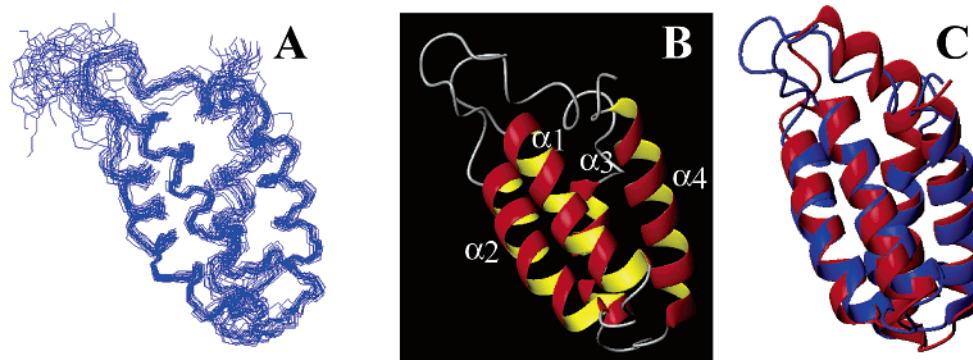


FIGURE 1: Solution structure of FRB. (A) Superposition of the backbone atoms of FRB structures. (B) One representative conformer of the NMR ensemble. (C) Comparison of the FRB solution structure (one representative conformer) (blue) and the crystal structure (PDB entry 1AUE) (red).

in the same location as rapamycin, *in silico* virtual screening was carried out using FlexX (17) as implemented in Sybyl (TRIPOS, Inc.). This process consisted of an initial round whereby 30 000 compounds (Chembridge, Inc., San Diego, CA) were docked. From these results, a second round evaluated several hundred of the highest-scoring compounds to determine those that realistically fit in the FRB binding pocket with minimal molecular distortion. This resulted in a final group of 56 compounds that could conceivably bind FRB (see Materials and Methods). As the chemical shifts arising from NMR-active nuclei in a protein are largely influenced by the structure and chemical environment of the protein, the observation of spectral changes would provide definitive evidence of ligand binding (37). In particular, we used initially the ^1H NMR aliphatic region of the protein spectrum which is not normally populated by resonances from organic molecules. In fact, in our experience, small molecules, even when containing aliphatic chains, do not exhibit resonances below 1 ppm in their 1D ^1H NMR spectra. In any case, eventual overlap (in the <0.7 ppm region) between protein and compound resonances would be easily identified by measuring 1D ^1H spectra of the compounds. The advantage of this simple assay is that relatively low concentrations of unlabeled protein and relatively short measuring times are needed for a primary screen, when compared with those of traditional 2D ^{15}N – ^1H HSQC-based screens. The latter could subsequently be used as a secondary, confirmatory assay and for chemical shift mapping studies. As an example of this simple screening strategy, representative ^1H spectra of FRB are shown in Figure 2. Panel A is a control showing a portion of the ^1H aliphatic region of the spectrum of 50 μM FRB at 10 $^\circ\text{C}$ in the absence (black) and presence (red) of a molecule that does not bind FRB. It is clear from this comparison that the two spectra are effectively superimposable. Similar results are obtained with any of a number of nonbinding molecules. The results in the presence of 100 μM rapamycin are shown in Figure 2B, where the color coding is the same as in panel A. By using this simple screening technique, four compounds that consistently produced spectral changes indicative of binding to FRB were identified (Figure 2C and Table 2).

As mentioned above, to assess the affinity and mode of binding of these compounds to FRB, 2D ^1H – ^{15}N HSQC NMR spectra with ^{15}N -labeled FRB were recorded in the absence and presence of the ligands, with rapamycin serving as a control. In addition, to provide FRB ^{15}N – ^1H HSQC

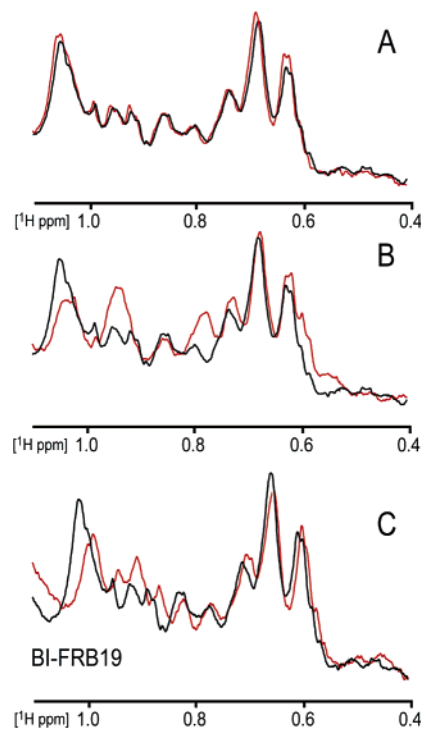
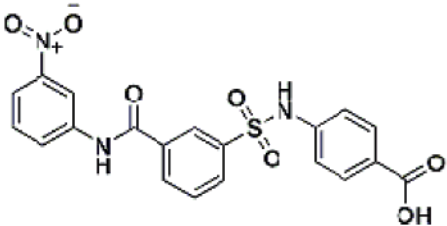
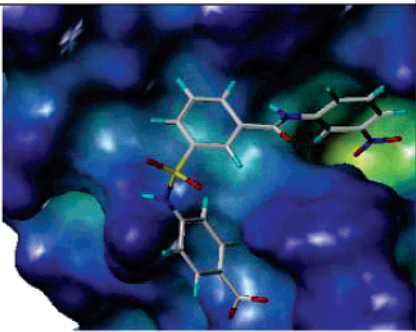
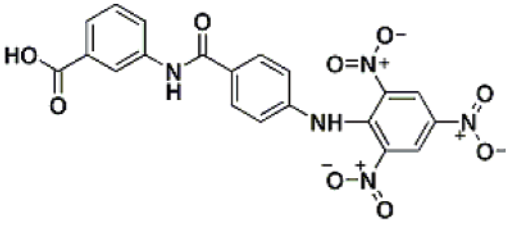
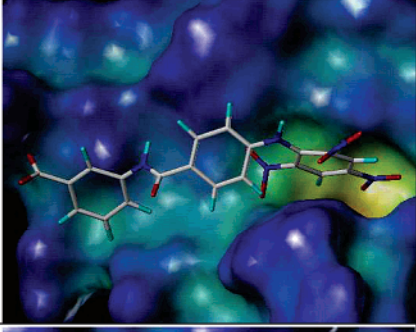
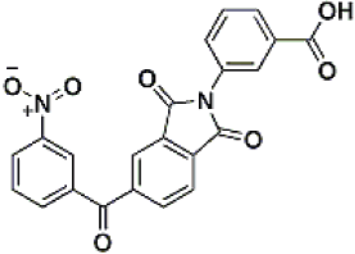
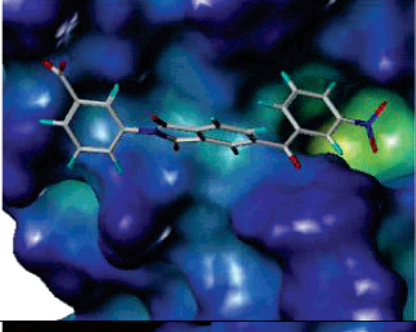
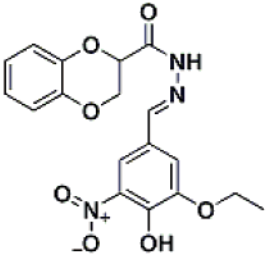
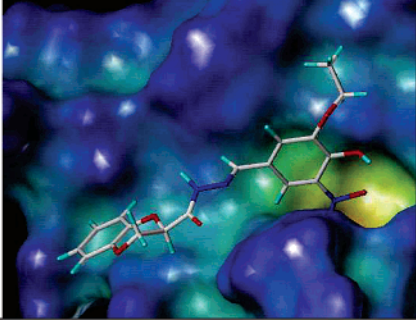


FIGURE 2: 1D ^1H NMR-based ligand screening. Panel A displays portions of the aliphatic regions from representative 1D ^1H NMR spectra of 50 μM FRB at 10 $^\circ\text{C}$ in the absence (black) and presence (red) of a ligand that does not bind FRB. Panel B displays similar portions of the aliphatic regions from 1D ^1H NMR spectra of 50 μM FRB at 10 $^\circ\text{C}$ in the absence (black) and presence (red) of 100 μM rapamycin. Panel C displays portions of the aliphatic regions from the 1D ^1H NMR spectra of 50 μM FRB at 10 $^\circ\text{C}$ in the absence (black) and presence (red) of the ligand BI-FRB19.

spectra that were relatively uncluttered, FRB was also prepared with selective ^{15}N [Gly and Ser labels. The Gly labeling was a direct consequence of using ^{15}N [Gly as the only source of ^{15}N . The Ser labeling came indirectly from scrambling of the labeled Gly, a common result when attempting selective Gly labeling. As it turned out, the presence of Ser peaks in the HSQC spectra did not interfere with the observed Gly peaks, and it helped in the backbone assignment because one Ser was initially unassigned.

A reference spectrum of FRB in the presence of rapamycin is shown at the left in Figure 3, where the black cross-peaks are for apo-FRB and the blue ones are for FRB in the presence of ligand (1:2 FRB/rapamycin ratio). There are clearly many major changes in the spectrum, as well as many

Table 2: Chemical and Docked Structures for the FRB Binders

	K_d	
BI-FRB10 	5 μ M	
BI-FRB19 	2 μ M	
BI-FRB19b 	2 μ M	
BI-FRB16 	100 μ M	

peaks that remain unaffected by the presence of rapamycin, indicating specific binding. In addition, using the resonance assignment, it can be determined that many of the peaks that have been affected are those that are in or near the known binding pocket. For example, it can be seen that the HSQC cross-peaks for residues G2040, S2035, A2034, F2039, R2036, and L2031 are significantly affected by complex formation. This agrees well with the X-ray crystal structure (14, 15) which specifically identifies several contacts between rapamycin and FRB, most of which involve the above-mentioned residues.

Figure 3 (middle panel) shows similar data for the ligand BI-FRB19 (Table 2). Again it is observed that there are many specific changes in the FRB spectra, most of which occur

for the same cross-peaks as in the presence of rapamycin. This is more clearly seen by overlaying the spectra of apo-FRB (black) with that of FRB in the presence of rapamycin (blue) or in the presence of BI-FRB19 (red) (Figure 3, right panel). Clearly, rapamycin and BI-FRB19 bind in the same location. Similar results are obtained upon addition of any of the ligands found to bind FRB listed in Table 2.

Subsequently, we performed NMR titrations of each ligand using ^1H – ^{15}N HSQC spectra of FRB. Titrations were carried out using samples of 100 μM [^{15}N]Gly-labeled FRB by following the chemical shifts of G2040. The change in the position of the G2040 cross-peak was monitored in both the ^1H and ^{15}N dimensions, and the chemical shift changes were calculated as a weighted average (δ_{avg}) of the changes as

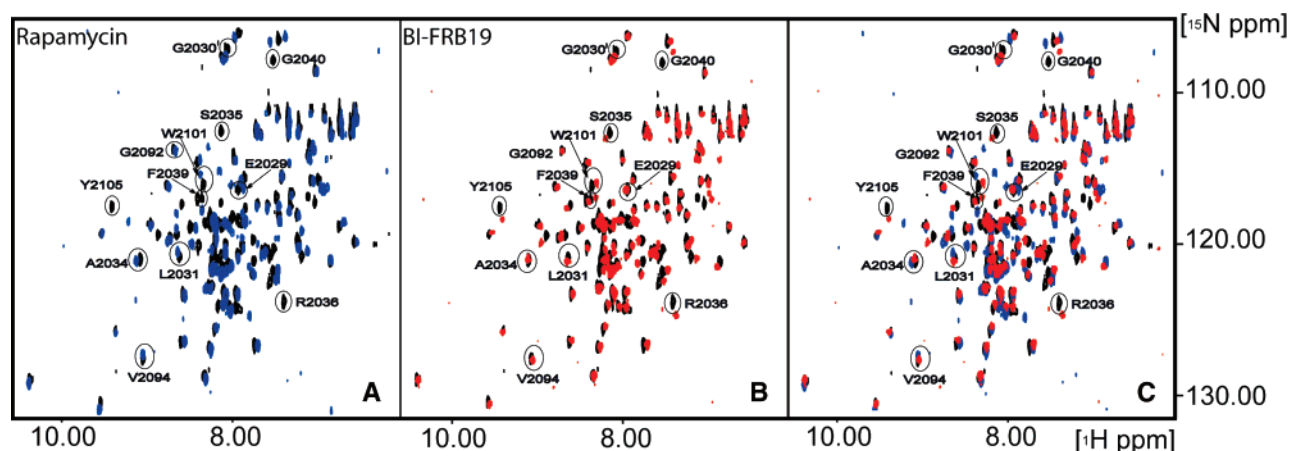


FIGURE 3: Results of chemical shift mapping of FRB in the presence of rapamycin or the ligand BI-FRB19. Panel A displays 2D ^1H – ^{15}N HSQC spectra of uniformly ^{15}N -labeled FRB (100 μM) in the absence (black) and presence (blue) of 200 μM rapamycin. Panel B displays similar results in the presence of 200 μM BI-FRB19 (red). Panel C displays the spectra of FRB in the absence (black) and presence of either rapamycin (blue) or BI-FRB19 (red).

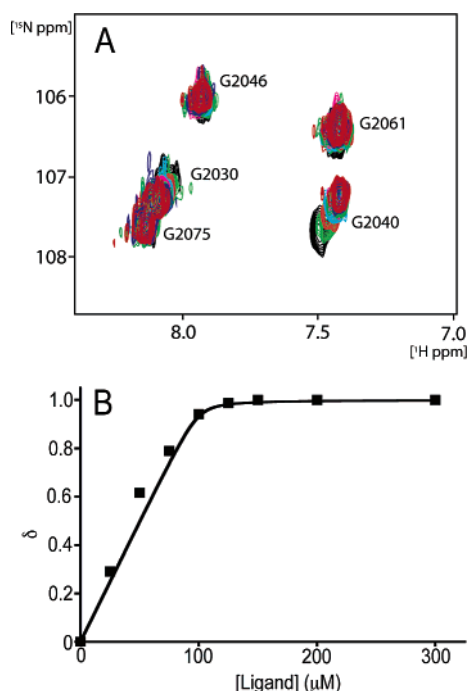


FIGURE 4: Determination of the dissociation constant by NMR. (A) 2D ^1H – ^{15}N HSQC spectra for a titration of ^{15}N -labeled FRB (100 μM) with the ligand BI-FRB19b. Concentrations of the ligand are as follows: 25 (green), 50 (orange), 75 (cyan), 100 (purple), 150 (dark green), 200 (purple), and 300 μM (red). (B) Plot of the normalized changes in chemical shift for the G2040 residue from panel A as a function of ligand concentration.

$\{[\delta^1\text{H}^2 + \delta(^{15}\text{N}/5)^2]/2\}^{0.5}$. These data were normalized and plotted as the fraction of the maximum observed change (δ_{max}) versus the concentration of ligand added.

HSQC-based NMR titrations are routinely used to measure K_d values (38). The results of such a titration for the ligand BI-FRB19b are reported in Figure 4. Panel A displays the Gly region of a series of ^1H – ^{15}N HSQC spectra of FRB as a function of an increasing ligand concentration. In Panel B is a plot of the fractional change in δ_{avg} versus ligand concentration. The results of a similar titration provide a K_d value of 2 μM for rapamycin. This value compares well with that recently reported in the literature of 26 μM (13) and with our kinase assay-determined IC_{50} value of 2.8 μM (see

below). The structures and K_d values of the strongest binding ligands of the 56 that have been tested are shown in Table 2.

A comparison of the ^1H – ^{15}N HSQC spectra acquired by using a uniformly ^{15}N -labeled FRB sample in the presence of different amounts of ligand (Supporting Information) shows that other peaks together with that of G2040 are significantly shifting. Analysis of these HSQC spectra and chemical shift variation of additional peaks give K_d values that are on the same order of magnitude as those reported.

Most of our ligands bind to FRB approximately as well as rapamycin, in the absence of FKBP12.

Evaluating the Biological Activity of FRB Ligands. While rapamycin action has been well characterized with in vivo and in vitro assays where FKBP12 is present, the effect of rapamycin in the absence of this protein is unclear. To address the potential biological function of rapamycin in the absence of FKBP12, we performed immune complex kinase assays with anti-mTOR immunoprecipitates and a GST–p70S6 kinase fusion protein that contains a known mTOR phosphorylation site, Thr389 (34). As previously described, incubation of immunoprecipitates with rapamycin in the presence of FKBP12 inhibits mTOR kinase activity in a concentration-dependent manner (Figure 5A). Surprisingly, incubation of immunoprecipitates with rapamycin alone also inhibited mTOR kinase activity with a calculated IC_{50} value of 2.8 μM (Figure 5B), which is in good agreement with our K_d value determined by NMR as well as the previously reported values (13). The kinase activity of a mTOR FRB mutant that does not bind rapamycin (S2035W) was unaffected by rapamycin, demonstrating that the effect of rapamycin alone still requires binding to the FRB domain of mTOR (data not shown). While we cannot formally rule out trace amounts of FKBP12 or another family member coprecipitating with mTOR, two lines of evidence make this a highly unlikely scenario. We have previously shown (39) that in pulldown experiments using a GST–FKBP12 fusion protein, binding of mTOR to FKBP12 in the absence of rapamycin was undetectable. In contrast, interaction between FKBP12 and mTOR was easily detected in the presence of rapamycin. In addition, both the Hall and Sabatini groups (40, 41) demonstrated similar results in co-immunoprecipi-

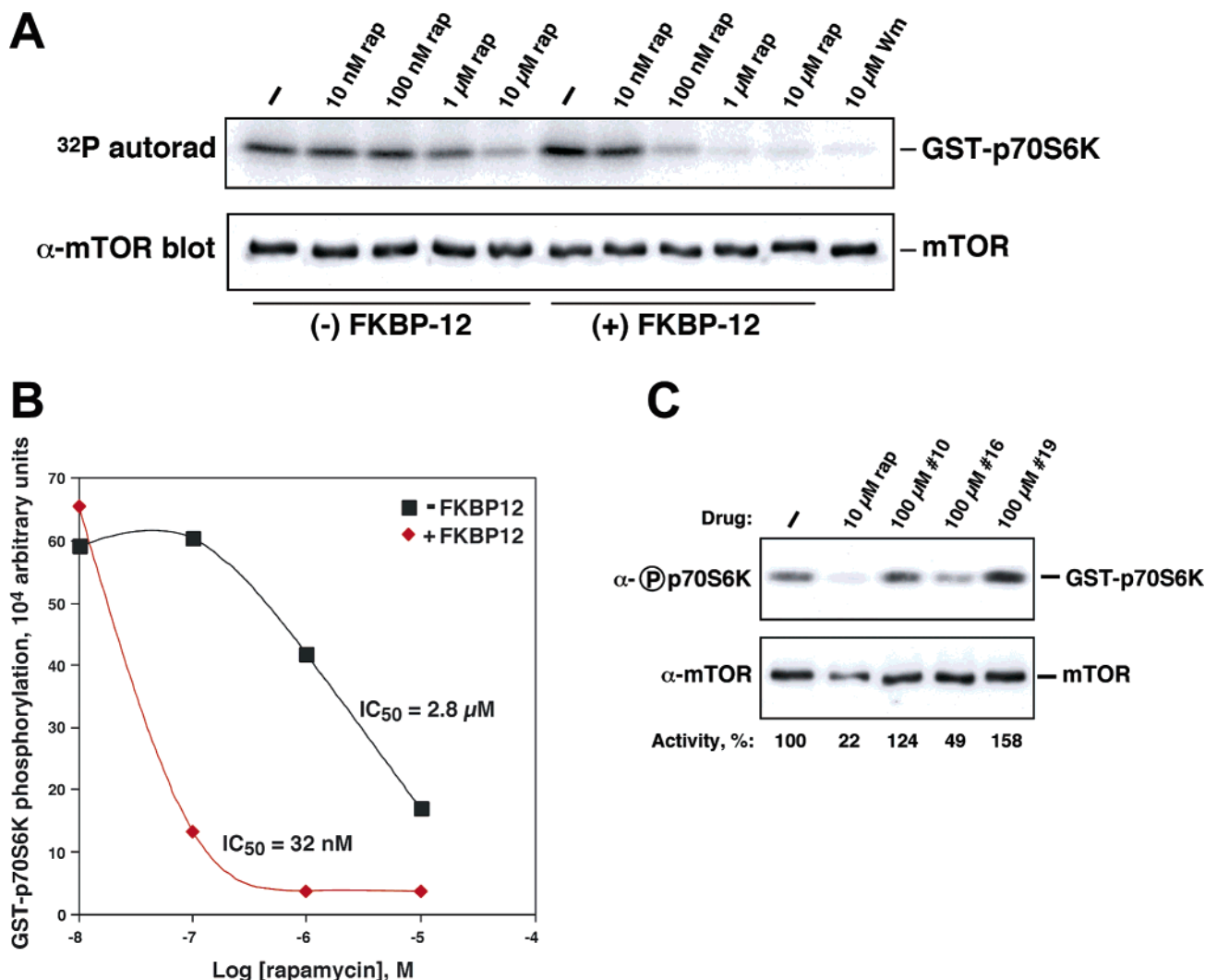


FIGURE 5: Inhibition of mTOR kinase activity. Panel A displays anti-mTOR immunoprecipitates that were incubated for 30 min with the indicated concentrations of rapamycin in the absence or presence of 1 μg of GST-FKBP12 protein. In the top row is the immune complex kinase assay with anti-mTOR immunoprecipitates and the GST-p70S6K protein as a substrate. Substrate phosphorylation was visualized with a PhosphorImager. In the bottom row, the same filter was immunoblotted with an anti-mTOR antibody. Wortmanin, an irreversible mTOR inhibitor (10 μM), was used as a positive control. Panel B is a quantitation of the in vitro kinase reactions with a PhosphorImager and densitometry. Calculated IC₅₀ values are shown in the plot. Panel C displays the results of the kinase assay performed in the presence of rapamycin and the FRB ligands BI-FRB10, BI-FRB16, and BI-FRB19.

tation experiments in which a transfected FKBP12 interacts with mTOR only in the presence of rapamycin. Therefore, the binding of rapamycin to mTOR in the absence of FKBP12 has an appreciable biological activity and allows for the possibility that any of the newly discovered FRB ligands may also exert similar inhibitory effects.

We tested three FRB ligands for their effect on mTOR kinase activity (Figure 5C). The results with these new ligands demonstrate some inhibition of mTOR kinase activity but with activity that is at least 10-fold weaker than the binding data. The best-performing ligand, BI-FRB16, reduces the level of phosphorylation of the GST-p70S6K fusion protein by $\sim 50\%$ at 100 μM . Conversely, the strongest binder, BI-FRB19, has no noticeable effect at all on p70S6K phosphorylation at 100 μM .

Possible competition between the ligands and rapamycin was also tested by first exposing mTOR immunoprecipitates to the ligand, followed by treatment with rapamycin prior to the immune complex kinase assay (data not shown). In all three cases, there was a significant reduction in the level

of p70S6K phosphorylation, similar to that of rapamycin alone, though in the presence of FRB19 the reduction was $\sim 60\%$. While there are many possible explanations for such an observation, this result is consistent with this ligand being able to compete with rapamycin for the same binding site.

Therefore, although these new ligands bind to the FRB domain, they appear to be substantially ineffective at inhibiting mTOR kinase activity. One possibility is that these ligands are too small and that some particular part of the rapamycin binding pocket must be bound for there to be appreciable inhibition. Another possibility is that the bulkier rapamycin structure may block the binding of an allosteric modulator of mTOR function, whereas the smaller molecules may bind in the pocket but fail to effectively block the binding of the modulator. These data therefore demonstrate that the small molecule binders we have identified uncouple FRB binding from inhibition of the catalytic domain of mTOR and may therefore prove to be useful in deciphering the function and complex regulation of mTOR in the cell.

CONCLUSIONS

We report here on the NMR resonance assignments and complete structure determination of the FRB domain of mTOR. By using NMR-based methods and in vitro kinase activity assays, we have demonstrated that rapamycin is able to bind its final target, the FRB domain, even in the absence of its in vivo binding partner, FKBP12, and that it still inhibits the kinase activity of mTOR with an IC_{50} value that is comparable with its dissociation constant to the FRB domain. In addition, we have identified several novel FRB ligands by a combination of virtual screening and NMR spectroscopy. The binding affinities of these ligands have been determined by NMR spectroscopy, and an initial investigation demonstrated that the most potent ligands (BI-FRB10 and BI-FRB19) could not significantly inhibit the phosphorylation of the mTOR substrate p70S6K, albeit they bind to FRB with an affinity similar to that of rapamycin in the absence of FKBP12. One compound, BI-FRB16, is capable of both binding to FRB and inhibiting the kinase activity of mTOR, although at higher concentrations. While the molecular bases for the inhibition of the kinase activity by rapamycin remain unclear, each of the proposed FRB ligands may serve as a scaffold for future inhibitor development, as well as providing additional tools to aid in elucidating the complex cellular signaling pathways where mTOR is involved.

ACKNOWLEDGMENT

We thank Professor Jie Chen (University of Illinois, Urbana, IL) for the kind donation of purified FRB for use in the initial experiments and for the pGEX-2T FRB construct used for expressing the isotopically labeled FRB.

SUPPORTING INFORMATION AVAILABLE

1H , ^{13}C , and ^{15}N chemical shifts of the FRB domain of mTOR measured at 283 K and a comparison of 1H – ^{15}N HSQC spectra of a ^{15}N -labeled FRB sample in the presence of 25 and 200 μM FRB19b. This material is available free of charge via the Internet at <http://pubs.acs.org>.

REFERENCES

- Wullschlegel, S., Loewith, R., and Hall, M. N. (2006) TOR Signaling in Growth and Metabolism, *Cell* 124, 471–484.
- Keith, C. T., and Schreiber, S. L. (1995) PIK-related kinases: DNA repair, recombination, and cell cycle checkpoints, *Science* 270, 50–51.
- Kunz, J., Henriquez, R., Schneider, U., Deuter-Reinhard, M., Movva, N. R., and Hall, M. N. (1993) Target of rapamycin in yeast, TOR2, is an essential phosphatidylinositol kinase homolog required for G_1 progression, *Cell* 73, 585–596.
- Anthony, J. C., Anthony, T. G., Kimball, S. R., and Jefferson, L. S. (2001) Signaling Pathways Involved in the Translational Control of Protein Synthesis in Skeletal Muscle by Leucine, *J. Nutr.* 131, 856S–860S.
- Barbet, N. C., Schneider, U., Helliwell, S. B., Stansfield, I., Tuite, M. F., and Hall, M. N. (1996) TOR controls translation initiation and early G_1 progression in yeast, *Mol. Biol. Cell* 7, 25–42.
- Gingras, A. C., Raught, B., and Sonenberg, N. (2001) Regulation of translation initiation by FRAP/mTOR, *Genes Dev.* 15, 807–826.
- Heitman, J., Movva, N. R., and Hall, M. N. (1991) Targets for Cell Cycle Arrest by the Immunosuppressant Rapamycin in Yeast, *Science* 253, 905–909.
- Beck, T., Schmidt, A., and Hall, M. N. (1999) Starvation Induces Vacuolar targeting and Degradation of the Tryptophan Permease in Yeast, *J. Cell Biol.* 146, 1227–1238.
- Albig, A. R., and Decker, C. J. (2001) The Target of Rapamycin Signaling Pathway Regulates mRNA Turnover in the Yeast *Saccharomyces cerevisiae*, *Mol. Biol. Cell* 12, 3428–3438.
- Hidalgo, M., and Rowinsky, E. K. (2000) The rapamycin-sensitive signal transduction pathway as a target for cancer therapy, *Oncogene* 19, 6680–6686.
- Vogt, P. K. (2001) PI 3-kinase, mTOR, protein synthesis and cancer, *Trends Mol. Med.* 7, 482–484.
- Dudkin, L., Dilling, M. B., Cheshire, P. J., Harwood, F. C., Hollingshead, M., Arbuck, S. G., Travis, R., Sausville, E. A., and Houghten, P. J. (2001) Biochemical correlates of mTOR inhibition by the rapamycin ester CCI-779 and tumor growth inhibition, *Clin. Cancer Res.* 7, 1758–1764.
- Banaszynski, L. A., Liu, C. W., and Wandless, T. J. (2005) Characterization of the FKBP-rapamycin-FRB ternary complex, *J. Am. Chem. Soc.* 127, 4715–4721.
- Choi, J., Chen, J., Schreiber, S. L., and Clardy, J. (1996) Structure of the FKBP12–Rapamycin Complex Interacting with the Binding Domain of Human FRAP, *Science* 273, 239–242.
- Liang, J., Choi, J., and Clardy, J. (1999) Refined Structure of the FKBP12–Rapamycin–FRB Ternary Complex at 2.2 Å Resolution, *Acta Crystallogr. D* 55, 736–744.
- Swindells, D. C. N., White, P. S., and Findlay, J. A. (1978) The X-ray crystal structure of rapamycin, *Can. J. Chem.* 56, 2491–2492.
- Rarey, M., Kramer, B., Lengauer, T., and Klebe, G. (1996) A fast flexible docking method using an incremental construction algorithm, *J. Mol. Biol.* 261, 470–489.
- Clark, R. D., Strizhev, A., Leonard, J. M., Blake, J. F., and Matthew, J. B. (2002) Consensus scoring for ligand/protein interactions, *J. Mol. Graphics Modell.* 20, 281–295.
- Gohlke, H., Hendlich, M., and Klebe, G. (2000) Knowledge-based scoring function to predict protein–ligand interactions, *J. Mol. Biol.* 295, 337–356.
- Eldridge, M. D., Murray, C. W., Auton, T. R., Paolini, G. V., and Mee, R. P. (1997) Empirical scoring functions: 1. The development of a fast empirical scoring function to estimate the binding affinity of ligands in receptor complexes, *J. Comput.-Aided Mol. Des.* 11, 425–445.
- Jones, G., Willett, P., Glen, R. C., Leach, A. R., and Taylor, R. (1997) Development and validation of a genetic algorithm for flexible docking, *J. Mol. Biol.* 267, 727–748.
- Forino, M., Jung, D., Easton, J. B., Houghton, P. J., and Pellecchia, M. (2005) Virtual docking approaches to protein kinase B inhibition, *J. Med. Chem.* 48, 2278–2281.
- Piotto, M., Saudek, V., and Sklenár, V. (1992) Gradient-tailored excitation for single-quantum NMR spectroscopy of aqueous solutions, *J. Biomol. NMR* 2, 661–665.
- Kay, L. E., Keifer, P., and Saarinen, J. T. (1992) Pure absorption gradient enhanced heteronuclear single quantum correlation spectroscopy with improved sensitivity, *J. Am. Chem. Soc.* 114, 10663–10665.
- Muhandiram, D. R., and Kay, L. E. (1994) Gradient-enhanced triple-resonance three-dimensional NMR experiments with improved sensitivity, *J. Magn. Reson., Ser. B* 103, 203–216.
- Talluri, S., and Wagner, G. (1996) An optimized 3D NOESY-HSQC, *J. Magn. Reson.* 112, 200–205.
- Zhang, O., Kay, L. E., Olivier, J. P., and Forman-Kay, J. D. (1994) Backbone 1H and ^{15}N resonance assignments of the N-terminal SH3 domain of drk in folded and unfolded states using enhanced sensitivity pulsed field gradient NMR techniques, *J. Biomol. NMR* 4, 845–858.
- Kumar, A., Ernst, R. R., and Wüthrich, K. (1980) A two-dimensional nuclear Overhauser enhancement (2D NOE) experiment for the elucidation of complete proton–proton cross-relaxation networks in biological macromolecules, *Biochem. Biophys. Res. Commun.* 95, 1–6.
- Bartels, C., Xia, T., Billeter, M., and Wüthrich, K. (1995) The program XEASY for computer-supported NMR spectral analysis of biological macromolecules, *J. Biomol. NMR* 5, 1–10.
- Güntert, P., Mumenthaler, C., and Wüthrich, K. (1997) Torsion angle dynamics for NMR structure calculation with the new program DYANA, *J. Mol. Biol.* 273, 283–298.

31. van Gunsteren, W. F., and Berendsen, H. J. C. (1990) Computer Simulation of Molecular Dynamics: Methodology, Applications and Perspectives in Chemistry, *Angew. Chem., Int. Ed.* 29, 992–1023.
32. Koradi, R., Billeter, M., and Wüthrich, K. (1996) MOLMOL: A program for display and analysis of macromolecular structures, *J. Mol. Graphics* 14, 29–32.
33. Laskowski, R. A., Rullmann, J. A., MacArthur, M. W., Kaptein, R., and Thornton, J. M. (1996) AQUA and PROCHECK-NMR: Programs for checking the quality of protein structures solved by NMR, *J. Biomol. NMR* 8, 477–486.
34. Chiang, G. G., and Abraham, R. T. (2004) Determination of the catalytic activities of mTOR and other members of the phosphoinositide-3-kinase-related kinase family, *Methods Mol. Biol.* 281, 125–141.
35. Veverka, V., Lennie, G., Crabbe, T., Bird, I., Taylor, R. J., and Carr, M. D. (2006) NMR Assignment of the mTOR Domain Responsible for Rapamycin Binding, *J. Biomol. NMR* (in press).
36. Odagaki, Y., and Clardy, J. (1997) Structural Basis for Peptidomimicry by the Effector Element of Rapamycin, *J. Am. Chem. Soc.* 119, 10253–10254.
37. Pellecchia, M., Sem, D. S., and Wüthrich, K. (2002) NMR in drug discovery, *Nat. Rev. Drug Discovery* 1, 211–219.
38. Shuker, S. B., Hajduk, P. J., Meadows, R. P., and Fesik, S. W. (1996) Discovering high-affinity ligands for proteins: SAR by NMR, *Science* 274, 1531–1534.
39. Edinger, A. L., Linardic, C. M., Chiang, G. G., Thompson, C. B., and Abraham, R. T. (2003) Differential effects of rapamycin on mammalian target of rapamycin signaling functions in mammalian cells, *Cancer Res.* 63, 8451–8460.
40. Jacinto, E., Loewith, R., Schmidt, A., Lin, S., Ruegg, M. A., Hall, A., and Hall, M. N. (2003) Mammalian TOR complex 2 controls the actin cytoskeleton and is rapamycin insensitive, *Nat. Cell Biol.* 6, 1122–1128.
41. Sarbassov, D. D., Ali, S. M., Kim, D. H., Guertin, D. A., Latek, R. R., Erdjument-Bromage, H., Tempst, P., and Sabatini, D. M. (2004) Rictor, a novel binding partner of mTOR, defines a rapamycin-insensitive and raptor-independent pathway that regulates the cytoskeleton, *Curr. Biol.* 14, 1296–1302.

BI060976+